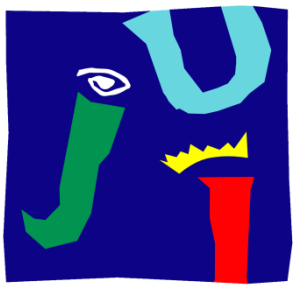

UNIVERSITAT JAUME·I

Escola superior de Tecnología i Ciències Experimentals

MASTER'S THESIS

USE OF CdS QUANTUM-DOTS FOR MINE WATER TREATMENT

Lucía Navarro López

Directed by: Dr. Francisco Fabregat Santiago

Castellón, July 2016

Master's Degree in Applied Physics

USE OF CdS QUANTUM-DOTS FOR MINE WATER TREATMENT

“*I have no special talent. I am only passionately curious*”

Albert Einstein

Acknowledgements

I would like to thank all those who work in the Group of Photovoltaic and Optoelectronic Devices (GDFO) at Universitat Jaume I, I have need, in special to Prof. Juan Bisquert director of the Institute of Advanced Materials (INAM), for the opportunity to realise my final thesis master in his group.

I would like to give a special thanks to Dr. Francisco Fabregat Santiago, my supervisor, for giving me the opportunity to work on this interesting subject, for his guidance, motivation, all interesting discussions and support that made possible this thesis.

I would also like to thank Elena Mas Marzá for her assistance, advice and all her help during the preparation of this work both inside and outside of laboratory.

This work could not have been possible without the support of Isaac Herraiz, Rafael Sánchez and Isaac Zarazúa, with their help in every moment that I needed.

I cannot forget to thank my co-workers, especially Bruno Clasen, Marta Vallés, Drialys Cárdenas and Nuria Vicente, for making the day-to-day more enjoyable. ♥

Most importantly, thanks to my mother Ana López, my father Jesús Navarro and my sister Gloria Navarro none of this would have been possible without the love and patience of my family. They have helped and encouraged me.

To *Serveis Centrals* at UJI, where structural, morphological and chemical characterizations were done.

Finally, I appreciate *SEFIN* association and *BioEletroMet* project for the financial support of this work.

Index

List of figures

List of tables

List of abbreviations

a	Absorptance
A	Absorbance
CB	Conduction Band
CE	Counter Electrode
CL	Compact Layer
CV	Cyclic Voltammetry
EIS	Electrochemical Impedance Spectroscopy
EQE	External Quantum Efficiency
FF	Fill Factor
FTO	Fluorine doped Tin Oxide
IC	Ion Chromatography
ICP	Inductively Coupled Plasma
IPCE	Incident Photocurrent Conversion Efficiency = EQE
IQE	Internal Quantum Efficiency
J	Current density
J_{sc}	Short Circuit current density
JV	Current density-Voltage
MFC	Microbial Fuel Cell
P_{max}	Maximum power
QDs	Quantum Dots
SEM	Scanning Electron Microscopy

SILAR	Successive Ionic Layer Adsorption and Reaction
PEC	PhotoElectroChemical cell
R	Reflectance
RE	Reference Electrode
T	Transmittance
VB	Valence Band
V_{oc}	Open Circuit Voltage
WE	Working Electrode

Abstract

A large amount of tailing water is generated from mines around the world every day. Tailing water requires adequate procedures to reduce its toxicity and, if feasible, to recover metallic ions present in its. This work describes a novel low cost, high performance photoelectrochemical system based on titanium dioxide photoanodes sensitized with CdS quantum dots that carry out Cu recovery and sulfur treatment of mine tailings simultaneously. Excitation of QDs by solar light promotes hole transfer to soluble sulfates and thiosulfates, while photogenerated electrons travel to a counter electrode where they reduce copper and facilitate its recovery. Under 1000 $W \cdot m^{-2}$ illumination, a maximum short-circuit current density of 7.4 $A \cdot m^{-2}$ was achieved meaning a copper recovery rate of 8.6 g $m^{-1} \cdot h^{-1}$. At the same time the device provided the highest open circuit potential of 1.13 V and a maximum power density of 3.0 $W \cdot m^{-2}$, one order of magnitude higher than that provided by microbial fuel cells in wastewater decontamination systems.

Aim and objectives

The contamination of water with heavy metals is considered the major problem in mining areas. In order to avoid this problem, in this work it is proposed the use of a photoanode, that under illumination, oxidizes sulfur species from mining wastewaters, and uses the electrons obtained in this process to recover metallic ions on the cathode. Furthermore, the complete system produces energy instead of consuming it.

Work structure

This work has been organized in five different sections. First, *Introduction* section describes the problems of water contamination in copper minery, different forms to remove metallic ions from water, an overview about main properties of semiconductors and quantum dots and some of their applications. Following, all the experimental procedures are explained in *Experimental section*, paying special attention to the different experimental techniques employed. Next, *Results and discussion*, discusses the main goals and outcomes achieved. Subsequently, the conclusion extracted from the experiments and studies performed are presented in *Conclusions* section. Finally, the last section, *References,* is devoted to all references included in this work.

Chapter 1: Introduction

Water is one of the most abundant resources on Earth and key for life. However, less than 1% of the water present in our planet is safe for human consumption.[1] Nowadays, different human activities, including mining and metallurgy, lead on to the production of millions of tons of wastewater per year, which contain toxic substances as heavy metals (copper, nickel, cobalt, zinc,[2] lead, arsenic[3]) and acid-generating sulfidic species, which are generally known as tailings. In general, tailings are defined as the materials left over after the process of separating the valuable fraction from the worthless fraction of an ore. These materials are suspended or dissolved in water, provoking its contamination. Heavy metals are normally present in tailing water in form of ions. The inadequate management and disposal of these mining wastes has a huge environmental impact, contributing to the pollution of groundwater (aquifers) and surface water (rivers and lakes). Consequently, this situation leads to a reduction of the amount water that can be used by humans and wildlife.

Copper can be found in food, water and air. This element is essential for human health; however an excess concentration can provoke serious health problems, such as anaemia, infertility or fungal infections. Besides, copper can also produce nervous system dysfunctions like depression, anxiety, obsessive-compulsive disorder, bipolar disorder, schizophrenia, etc.[4]

Cooper is one of the metals with more extended use worldwide, mainly due to its applications in communications, energy transport, engineering and architecture. In the recent past, rich ore mining procedures have been stressed to satisfy worldwide demand of cooper. This fact has yielded to explore the use of low grade ore and mine waste as alternative source to produce copper metal. Bioleaching has been successfully combined with electro-wining (electrodeposition) with this purpose, providing today about 20 % of world copper. Unfortunately this procedure produces larger amounts of tailing water and consumes a greater amount of energy than classical minery.

The directive 2006/44/EC of the European parliament and of the council of 6th September 2006 on the quality of fresh waters,[5] established the maximum

concentration of dissolved copper (mg/L Cu) allowed for different water hardness values, as shown in Table 1.

Table 1. Maximum concentration of dissolved copper allowed in fresh water for different water hardness

Water hardness (mg/L $CaCO_3$)	10	50	100	300
mg/L Cu	0.005[(1)]	0.022	0.0	0.112

[(1)] Presence of fish in waters containing higher concentrations of copper may indicate a predominance of dissolved organo-cupric complexes.

In order to eliminate or recover heavy metals from tailings, both chemical-physical and electrical methods are employed.

The most commonly used chemical-physical methods to recover metals are:

- *Chemical precipitation* is an expensive procedure which requires the use of chemicals. Metals such as copper, zinc, iron, manganese, nickel, and cobalt can be recovered by precipitation with hydroxide.[6]

- *Cementation* is a metal precipitation from aqueous solution, which occurs due to the presence of another metal. In this process the metal is deposited or precipitated usually "cemented" onto the metal added.[7]

- *Ultrafiltration* consists in using semipermeable membranes that act as “molecular sieves” allowing the pass of soluble compounds through their pores.[8]

- *Solvent extraction,* in this method the metal is extracted form an aqueous solution by a ‘liquid-liquid’ extraction with an organic solvent. When needed, the metal ion is previously reacted with the appropriate chemical to favour its solubility in the organic phase.

- *Adsorption* of the metal ion by using activated carbon or resin-in-pulp.

Among the electrical procedures, the most commonly used are electrodeposition, bioelectrochemical deposition and the novel performance proposed in this work photoelectrochemical metal recovery:

- *Electrodeposition of metals*, also named electro-wining, consumes electricity to recover bulk metals from tailings with high purity. This procedure is widely used in metallurgical processing and treatment of waste streams. In the particular case of

tailings water containing different metals, a selective metal recovery is possible when the metals present different reduction potential.[6]

- *Bioelectrochemical metal recovery*, this procedure mainly consists in the use of Microbial Fuel Cells (MFCs), which are bioelectrical systems based on the use of bacteria to generate the current needed for metal electrodeposition. Although this procedure has already been described for the recovery of copper, present efficiencies are very low (over 1.5 $A \cdot m^{-2}$.)[9-11] Figure 1 shows a MFC used for cooper recovery. As it can be observed, bacteria at the anode produce a biological oxidation of an organic compound and deliver electrons to the cathode where copper ions are reduced to copper metal. MFCs are more efficient than other electrical-based processes for metal recovery, mainly because electricity is produced instead of being consumed.

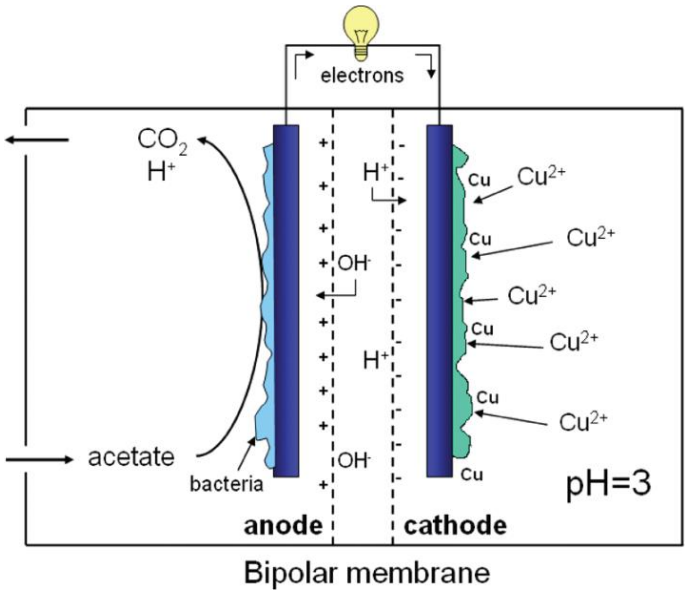

Figure 1. Principle of a MFC for copper reduction.

- *Photoelectrochemical metal recovery*: Photoelectrochemical processes transform light into energy, through several processes that start with the electron excitation after the absorption of one photon (photoexcitation). PhotoElectroChemical cells (PECs) consist of semiconductor photoanodes and/or photocathodes which absorb incident sunlight and use the photogenerated electron-hole pairs to carry out oxidation and reduction reactions respectively at the electrode-electrolyte interface. Wide-bandgap inorganic semiconductors, namely the system of Titanium dioxide nanoparticles sensitized with CdS/CdSe/PbS quantum dots (QDs) have already been investigated extensively for solar water splitting purposes,[12,13,14] but never before for water treatment.

1.1. Semiconductors

Over the last 70 years, semiconductors have become the most important material for the fabrication of electronic and optoelectronic devices. There are different definitions of semiconductor. Historically a “semiconductor” was used to indicate materials with higher conductivity than insulators, which possess lower conductivity than metals measured at room temperature. But this definition is not complete as, for example a semiconductor can be transformed into an insulator at very low temperatures.[15]

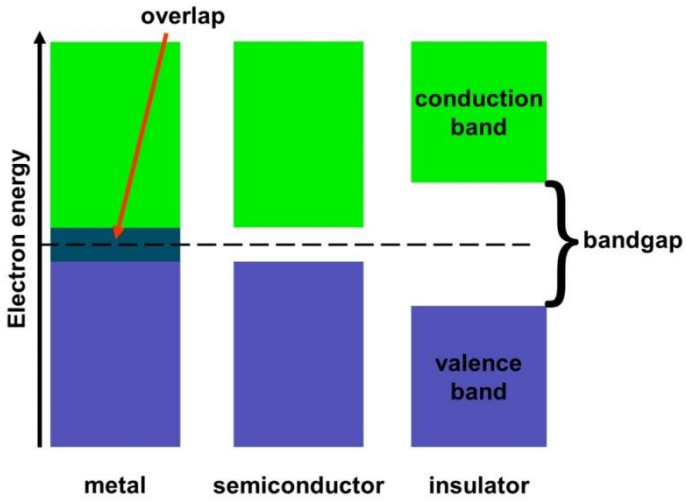

Figure 2. Position of conduction band and valence band in metals, semiconductors and insulators.

A general classification of the materials according to their electrical properties define: (i) The metals are materials in which there is an overlap between the conduction band (CB) and valence band (VB) as it is shown in Figure 2 (left). No bandgap is defined for metals. (ii) Insulators, there is a wide bandgap between the bands (>3.5eV) and therefore, electrons cannot be promoted easily from the VB to the CB, see Figure 2 (right). (iii) Semiconductors have a bandgap width between conductors and insulators (i. e. between 0.5 and 3.5eV), the VB is full of electrons and the CB is practically empty. In semiconductors, electrons can be promoted to the CB through the bandgap using a photon with relatively small energy (but higher than the bandgap energy).

1.2. Quantum dots

In 1932, H. P. Rocksby discovered that the colour of some silicates glasses is linked to microscopic composition of CdSe and CdS,[16] but it was in 1985 when these changes of colour were associated to the energy states determined by quantum confinement in these CdSe and CdS.[17] From that moment, the experimental studies about quantum dots (QDs) have been developed very fast. Figure 3 illustrates the increased interest in QDs.

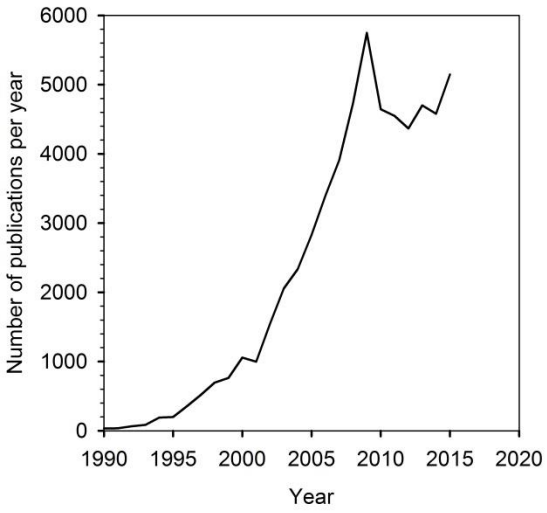

Figure 3. Increase of publications on quantum dots.[18]

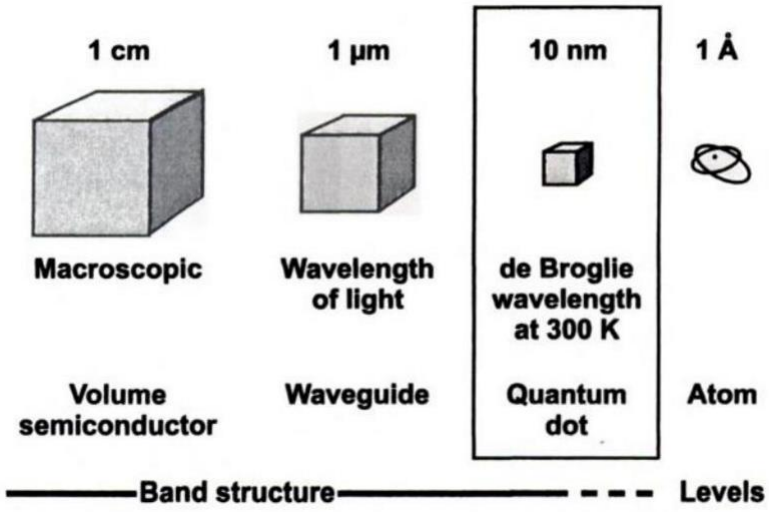

Figure 4. Schematic comparison of typical dimensions of bulk material, waveguides for visible light, quantum dots, and atoms.[19]

The term of “quantum dot” refers to crystalline structure of units of nanometers see Figure 4, which are formed by tens of thousands of atoms.

QDs are called “artificial atoms” because their energy levels present discrete confinement effect; i.e., due to the separation of energy levels, the electrical and optical properties can change as a consequence of the widen of the energy bandgap, as shown in Figure 5. In fact, the main advantage the use QDs in nanotechnology is the possibility of modifying properties without changing the material, which are assigned to a phenomenon called quantum confinement.[19, 20]

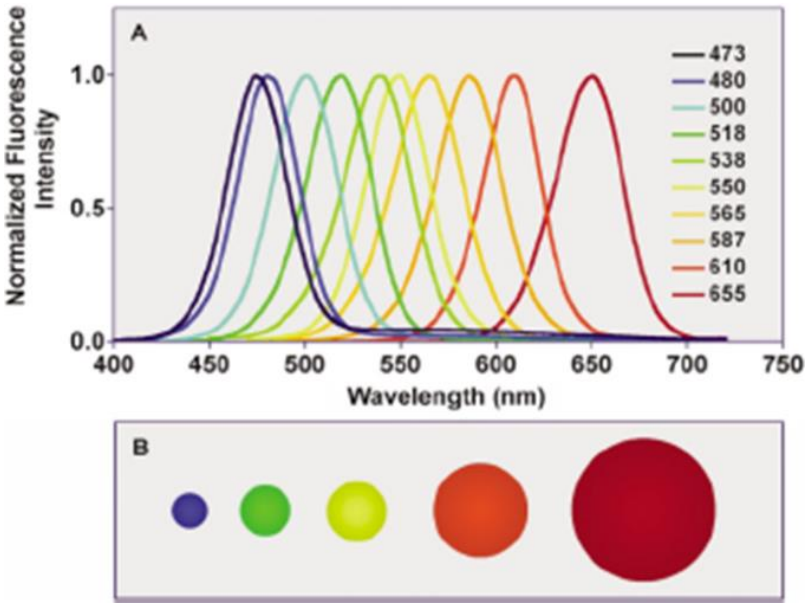

Figure 5. Variation of the position of the energy bandgap of a semiconductor material as a function of particle size.[21]

Another advantage of QDs is their high absorption coefficients,[22] which allows to obtain devices able to absorpt a higher number of photons using least amount of material. Furthermore, the final properties of quantum dots solar cells depends on the performance, such as preparation methods, surface defects, stability of compounds and photoelectronic characteristics or sensitization of TiO_2 photoanodes.[23]

There are several routes to synthesize the QDs. In this project, the "Successive Ion Layer Adsorption and Reaction" method (SILAR) has been applied to prepare the QDs (see Chapter 2 for experimental details).

1.2.1. Structure description of CdS/ZnS QDs

QDs can present different structures, including core,[24] core/shell or core/shell/shell. The difference in energy levels between the shell and the core determines the extraction of electron and/or holes from the core. Depending on the position of the energy levels, structures core/shell can be type I or type II, see Figure 6. In the case of type I-QDs, the electron-hole pair photogenerated stays on the core, whereas in case of type II-QDs, the shell allows that the photogenerated electrons or holes escape from the core. [25]

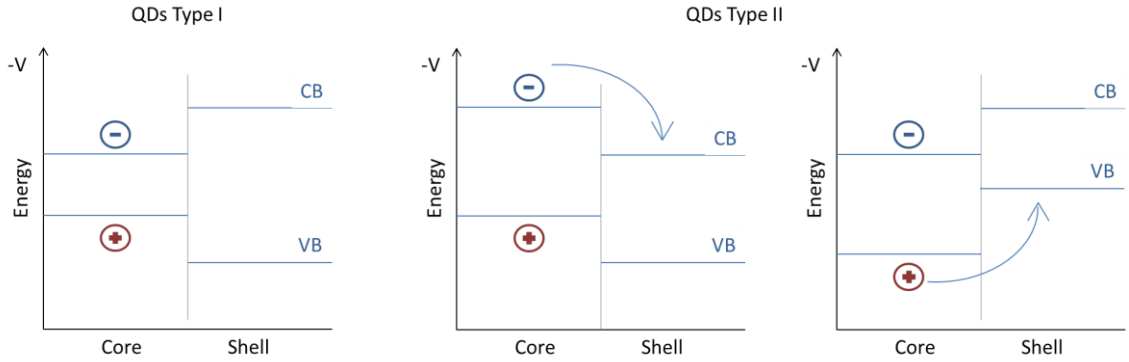

Figure 6. Schematic representation of the alignment of energy levels in different systems core/shell.

In this work the QDs under study are CdS+ZnS of type I, where the energy gap of the shell is bigger than the one of the core, thus leading to the confinement of the photogenerated electrons and holes in the core. In the final device, under working conditions, the electrons will be collected at the contact of the photoanode while holes will tunnel to the solution through the very thin ZnS layer.

The shell provides an optically active physical barrier between the core and the solution, in addition provides less sensitivity to environmental changes and chemical surface stabilization. The shell also passivates the surface states (“trap states”) of the core. Figure 7 shows the difference in energy levels of TiO_2, CdS and ZnS, as well as the states.

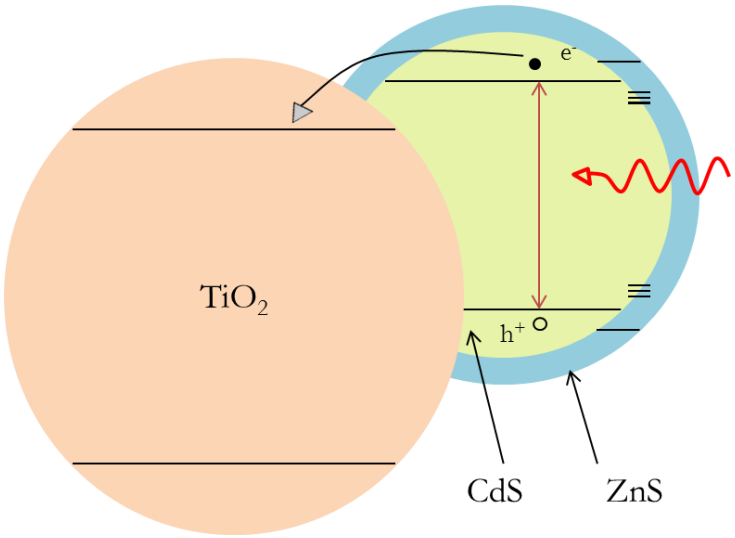

Figure 7. Energy levels from ZnS/CdS/TiO_2.

1.2.2. QDs applications

One of the main applications of QDs is in light emitting diodes (LEDs), principally due to the electroluminescent properties of QDs, as they can emit light after applying a voltage. QDs consume less power than conventional materials, therefore being appropriate for the fabrication of electronic devices. Furthermore, in contrast to conventional materials, QDs can also be used for the fabrication of flexible screens.

Another important application is the use of QDs as absorber materials in photovoltaic cells due to their high light absorption. Surely QDs will play an important role in the development of photovoltaic energy and optoelectronic devices.

QDs have also been employed in biomedical imaging. It is possible to use them for studying biological processes *in-vivo*, their small size makes possible introduce them in cells.

Chapter 2: Experimental methods

2.1. QDs preparation

All solvents and reagents were used as received from commercial suppliers without further purification.

Substrate preparation

TEC-15 Fluorine doped tin oxide (FTO) coated glass substrates from Pilkington with dimensions 25.0 x 12.5mm^2 and ~15Ω/sq. sheet resistance, were used as substrate. FTO was cleaned with soap (Extran® MA 02 neutral) and rinsed with deionised water for 15 minutes in an ultrasonic bath. Then, the substrates were sonicated for 15 minutes in a solution of ethanol absolute for 15 minutes and rinsed with acetone and dried with compressed air. After that the cleaned FTO substrates were treated in an ultraviolet-ozone system for 10 minutes.

TiO_2 compact layer

In specific samples, a TiO_2 compact layer (CL) was deposited onto the substrates by spray pyrolysis at 450^{0}C. The solution used for the deposition was titanium diisopropoxide bis(acetylacetonate) (75% in 2-propanol, Sigma-Aldrich) solution diluted in ethanol (1:39, v/v), with oxygen as gas carrier. After the spraying process the films were sintered on a hot plate at 450ºC for 5 minutes. After that, the substrates were cooling down to room temperature. The objective of the CL is double: blocking recombination of photogenerated electrons at FTO/electrolyte interface and enhancing electron contact between FTO and mesoporous TiO_2 film to improve the electron injection process.

The *spray pyrolysis technique* is a simple and relative cost-effective widespread method used to prepare films of any composition with different thickness, ceramic coatings and powders. This technique does not require high-quality substrates or chemicals. The spray pyrolysis equipment consists of an atomizer, precursor solution,

substrate heater and temperature controller. The solution that contains the compound to deposit is placed in the recipient connected to the atomizer. A carrier gas is necessary for transporting the solution and for its atomization. Flow meters are used to measure the flow of precursor solution and air. See Figure 8. The properties of the film obtained depend on the spray rate, temperature, atmosphere, carrier gas and cooling after deposition.[26]

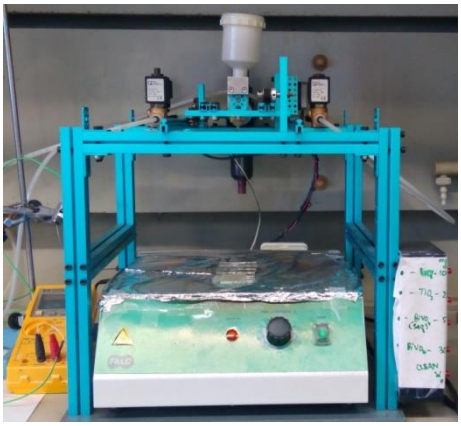

Figure 8. Spray pyrolysis equipment.

For this project, O_2 (g) was used as carrier gas. With an automatic spray pyrolysis machine, homogeneous depositions can be achieved, so this was the method used for the preparation of the TiO_2 CL.

Mesoporous TiO_2

A mesoporous TiO_2 layer was deposited by screen printing TiO_2 paste (Dyesol 18NRT, 20nm average particle size) and dried at 80ºC for 10 minutes. The different thicknesses were made doing different cycles in screen printing, drying each layer at 80 ºC for 10 minutes. Subsequently, the TiO_2 layers were heated at 500ºC for 30 minutes and cooled to room temperature. The thicknesses, determined by profilometry, were ~2.8, 5.8 and 8.2µm.

The *screen printing technique* consists of a synthetic fibre screen with a pattern framed. The screen, filled with a solution to be deposited, is placed near the substrate and then the squeegee draw linearly across the screen. At this point, the solution is deposited on the substrate drawing the screen pattern on the substrate see Figure 9 and Figure 10.

The thickness of the coated film is, in principle, given by the theoretical paste quantity on the screen. The characteristics of the film obtained can vary depending on the force with which squeegee is pushed into the screen, the snap-off distance, speed of the squeegee and the viscosity of the solution.[27]

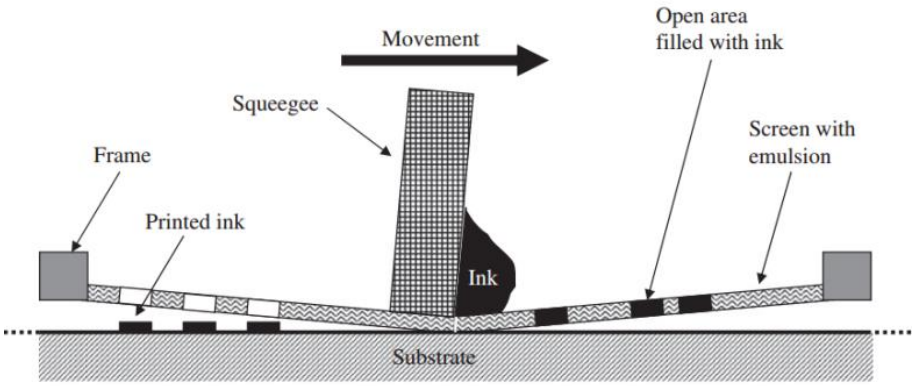

Figure 9. Illustration of the screen printing process.

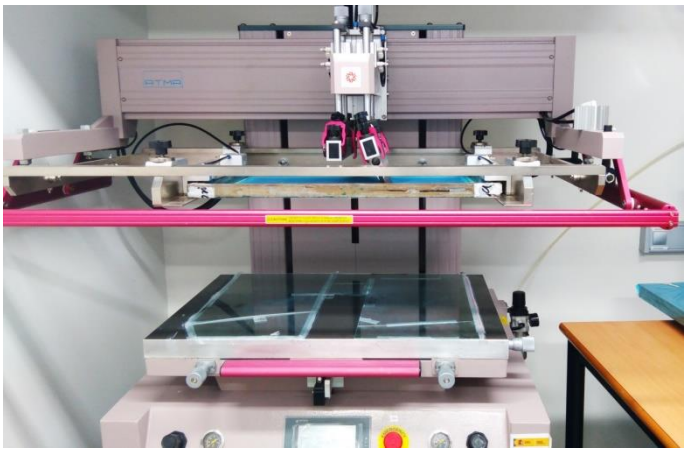

Figure 10. Screen printing system.

QDs deposition

This procedure is an appropriate method to prepare binary semiconductors QDs materials like CdS, CdSe, ZnS, PbS, etc. In this method, QDs are adsorbed on a substrate by dipping in different cationic and anionic solutions of the QDs precursors. Repeating cycles is possible to control the growth.[28]

The SILAR technique was used to grow a ZnS coated CdS quantum dot layer on top of the mesoporous TiO_2. The substrates were dipped into the ionic precursor solutions

for one minute, 5 cycles in CdS and 2 cycles in ZnS. In the case of CdS, 0.05M solution of $Cd(NO_2)_3$ (Sigma-Aldrich) in ethanol and 0.05M solution of $Na_2S{\cdot}9H_2O$ (Sigma-Aldrich) in methanol/deionised water (1:1, v/v) were used. For ZnS a 0.1M solution of $Zn(CH_3COO)_2$ (Sigma-Aldrich) and 0.1M solution of $Na_2S{\cdot}9H_2O$, both in deionised water, were used. After each dipping step, the electrodes were dipped in the same solvent in order to rinse the excess of precursor.

SILAR technique is based on sequential adsorption reactions of ions in solutions. The reaction between cations and anions forms the compound of the thin film deposited. This technique consists of the crystal growth “layer by layer” by sequentially dipping the substrates into the ionic precursor solutions. The adsorption is liquid-solid, being an exothermic process that implies forces of cohesion, Van-der-Waals or chemical attraction. Different factors, including temperature, pressure, type of substrate, surface area, concentration of solutions, etc. determines the film quality obtained. Figure 11 shows a representative graph of a SILAR process, where steps I and III are ionic precursor solutions adsorption and II and IV is the removal of excess of ion adsorbed. Figure 12 shows the SILAR equipment used.

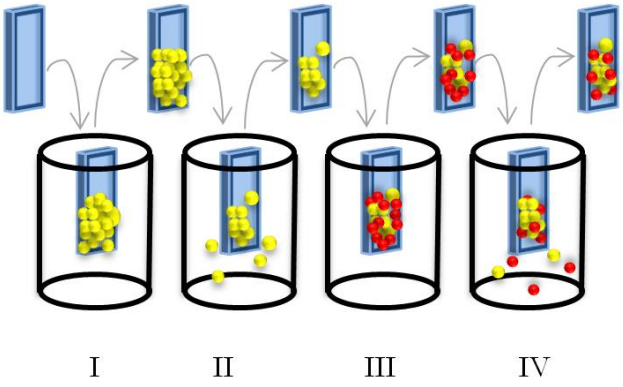

Figure 11. Representative diagram of SILAR process.

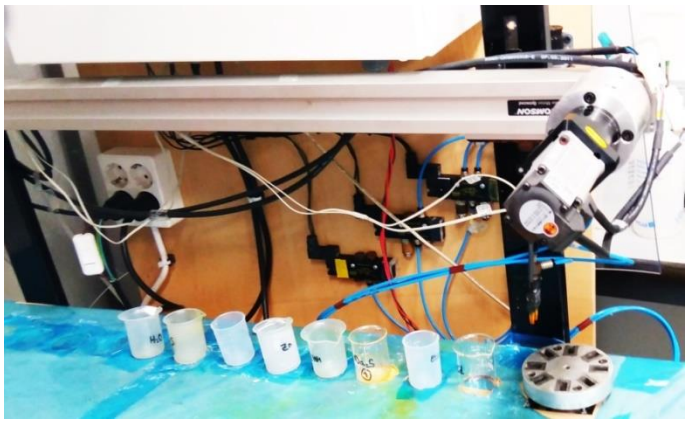

Figure 12. SILAR equipment.

2.2. Photoelectrochemical system

A scheme of the PEC used is shown in Figure 13. The operation of the cell is as follows: CdS QDs absorb light that excites electrons from VB to CB. Favoured by energy alignment, these electrons are injected to the CB of the mesoporous TiO_2 layer. From here, electrons are collected towards a wire and directed to the cathode where they reduce Cu^{+2} ions in solution to their metallic form. At the photoanode, the ionized QDs transfer the remaining hole to the different sulfur species present in the tailing water.

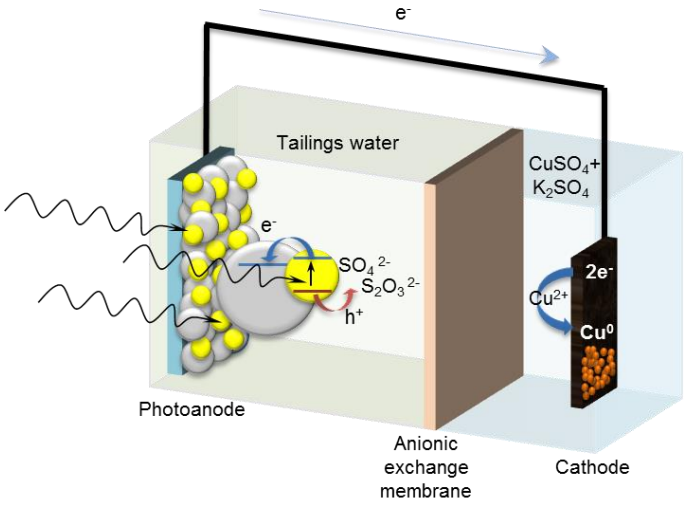

Figure 13. Photoelectrochemical cell.

Two electrode system

The photoactive anode, the working electrode (WE), is the mesoporous TiO_2 layer sensitized with CdS QDs described in previous section. The electrolyte at the photoanode side is tailing water (pH 13) whose composition is detailed in Table 2 of section 2.3. The counter electrode (CE) used was a graphite sample and its corresponding electrolyte was a $CuSO_4$ + K_2SO_4 solution with a Cu concentration of $1g \cdot L^{-1}$ and pH adjusted to 2 with H_2SO_4 and to a conductivity of $10mS \cdot cm^{-1}$ with K_2SO_4 to imitate typical tailing conditions. The system consisted in a two compartments cell separated using an anionic membrane which prevented the flow of Cu^{2+} ions from the CE side to the working electrolyte side.

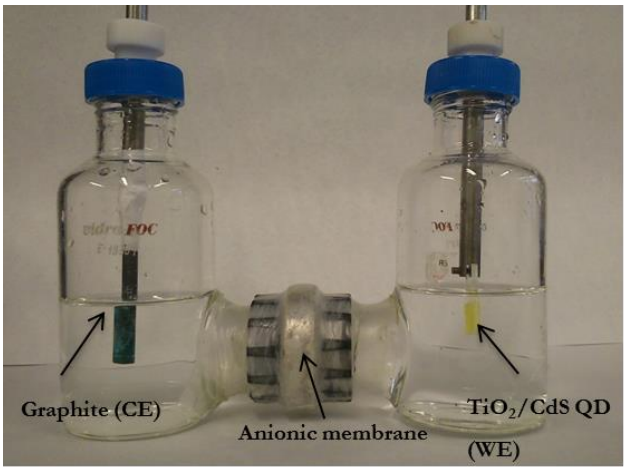

Figure 14. Two electrode PEC.

Three electrode system

In three electrode system, the photoactive anode was the WE the same as in previous section, the CE used was a platinum wire and the reference electrode (RE) was an Ag^+/AgCl (3M). To simplify the measurements, a single compartment cell, as the one shown in Figure 15, was used in these measurements. The electrolyte was tailing water (pH 13) whose composition is detailed in Table 2 of section 2.3.

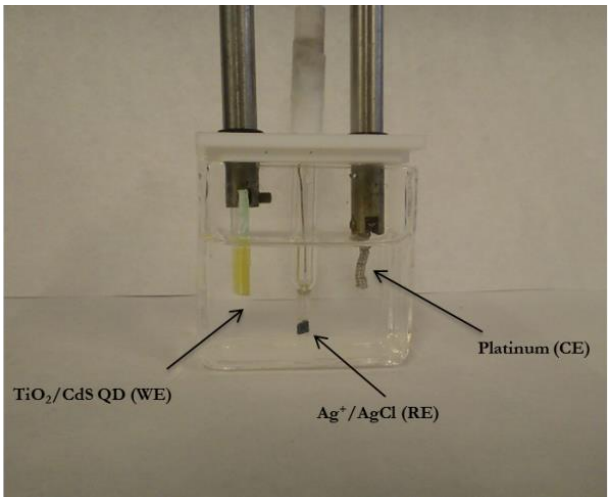

Figure 15. Three electrode cell.

2.3. Characterization

Electrochemical Impedance Spectroscopy

Electrochemical Impedance Spectroscopy (EIS) was used to identify the series resistance of the cell. EIS is a new technique which permits characterize electrical properties of a system.

The basis of this technique is to introduce a disturbance in the system and measure the response. A typical montage of this technique is an electronic circuit as shown in Figure 16. Being the symbol ~ the disturbance. In this work, the voltage applied was varied and the current measured.

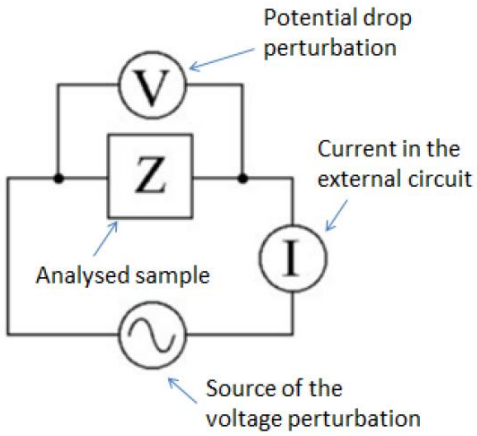

Figure 16. Scheme of impedance assemble.

The disturbance introduced in the system is in AC (alternating current); therefore it has a sinusoidal shape and has an associated frequency value. Knowing the frequency value of the input signal (f), the magnitude of perturbations amplitude to the voltage (V_m), delay time between them (τ), it is possible to calculate the impedance using Equation (1):

$$Z=\frac{V_m}{I_m}\cdot e^{i2\pi\tau f}=\frac{V_m}{I_m}\cdot e^{i\phi} \qquad (1)$$

Absorptance and Absorbance

Using a spectrophotometer Cary 300 UV-Vis Varian equipped with integrating sphere, reflectance (R) and transmittance (T) between 350 to 600nm were measured. From these measurements, both absorbance (A) and absorptance (a) could be calculated following Equation (2) and Equation (3) respectively:

$$A=-\log(T+R) \qquad (2)$$

$$a=1-T-R \qquad (3)$$

External Quantum Efficiency

External Quantum Efficiency (EQE), also called Incident Photocurrent Conversion Efficiency (IPCE), was measured by employing 300W Xe lamp coupled to a monocromator. The photoelectrode was polarized a desired voltage using and the photocurrent was measured using an optical powermeter 70310 from Oriel Instruments. A Si photodiode was used to measure the light intensity to calibrate the system. EQE was calculated following Equation 4:

$$EQE(\%)=\frac{I_{ph}(A)}{P_\lambda}\times\frac{1239.8(Vm)}{\lambda(nm)}\times 100 \qquad (4)$$

Where I_{ph} is the photocurrent, the value 1239.8 corresponds to the product hc (Plank's constant and speed of light, respectively), P_λ is the power of light at a particular wavelength and λ is the wavelength of irradiation.[29]

Structural characterization

The morphological structure and microanalysis were analysed using a Scanning Electron Microscope (SEM) JEOL 7001F equipped with an energy dispersive spectroscopy system INCA 350 (Oxford) and a wavelength dispersive system INCA Wave 200 (Oxford).

Tailings composition analysis

Tailing water was provided from Boliden (Sweden). Ion Chromatography (IC) and Inductively Coupled Plasma Mass Spectrometry (ICP), using ICP-MS Agilent 7500cx were used to determine the chemical composition of the tailing water.

Slight deviation found between the two measurement techniques is attributable to both accuracy in ICP measurements and precision associated to determination of K^+, Ca^+ and Na^+, which is often disturbed by the signal from other elements, especially at high cation concentration.

Very good agreement is found for sulfur measurements.

Table 2. ICP and IC analysis of tailing water.

Technique	Element	Average concentration [mg/L]+
ICP	Sodium	44.6
	Potassium	15.7
	Calcium	226
	Sulfur	257
IC	Na^+	57.8
	K^+	21.2
	Ca^{2+}	272
	Cl^-	12.3
	NO_3^-	12.7
	SO_4^{2-}	550
	$S_2O_3^{2-}$	138.3

Cyclic voltammetry

The behaviour of PECs is determined by cyclic voltammetry (CV) curves. CV is an electrochemical technique, which consists in applying a potential disturbance that has a linear variation with time between two voltage limits. In potentiostats, the current is measured between CE and working electrode (WE), while the voltage used to control and monitor data is the lecture between WE and RE. In two electrodes measurements RE is connected to CE.

Parameters such as short circuit current density (J_{sc}), Open Circuit Voltage (V_{oc}), maximum power (P_{max}) and Fill Factor (FF) were employed in order to analyse and optimized the devices. The two first parameters are directly obtained from the average

values given by CV's. Power (per unit area) is obtained from the product of the current density and potential (P = J·V), from which maximum value is taken. Finally, FF can be calculated following Equation 5.

$$FF = \frac{P_{max}}{V_{oc} \cdot J_{sc}} \qquad (5)$$

Ideally FF should approach a value 1, thus it is a parameter that describes how much the J-V curves deviates from a quasi-ideal rectangle and serves to evaluate internal inefficiencies of the cell, see Figure 17.

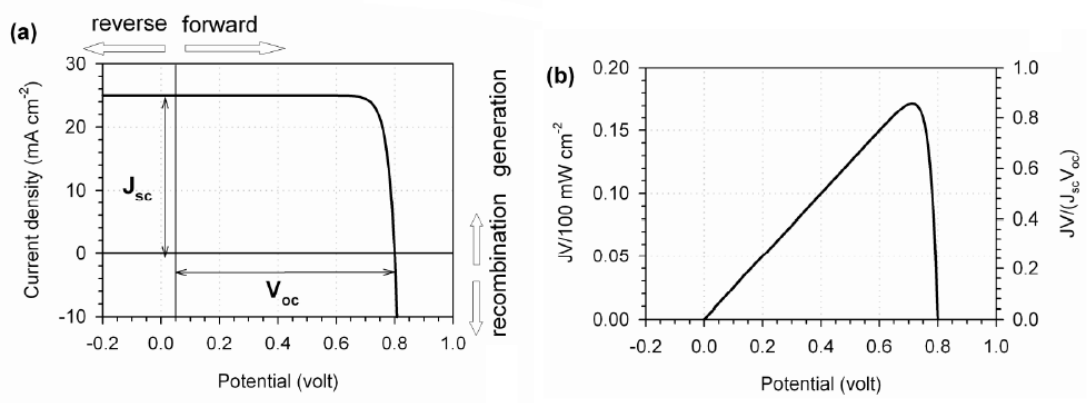

Figure 17. JV and power curve of short circuit.[30]

CV measurements were done under illumination using a 300W Xe lamp, where the light intensity was adjusted with a thermopile to 100mW cm^{-2} equivalent to standard AM 1.5G sunlight. The scan rate for CV measurements was 50mV·s^{-1}. Same experimental parameters were employed for chronoamperomety measurements, which were performed at 0.5V.

All the electrochemical measures were made in a potentiostat/galvanostat AUTOLAB under AM 1.5 (1 sun) illumination at room temperature

Chapter 3: Results and discussion

All the photoanodes studied in this work had the following configuration: FTO/TiO_2 CL/TiO_2 mesoporous/CdS-ZnS QDs.

3.1. Photoelectrochemical cell operation

Initially, in order to determine if the contribution to the photocurrent generated at the photoanodes was produced only from the QDs, a 3-electrode measurement were carried out with FTO/TiO_2 CL/TiO_2 mesoporous (8.2µm thick), with and without QDs. The measurements were performed in tailings, using platinum as cathode and Ag/AgCl (3M) as RE. As it can be observed in Figure 18 (a), negligible contribution from the FTO and the TiO_2 was detected, thus indicating that the photocurrent was produced by QDs. Furthermore, it was also checked which part of the photoanode, front (TiO_2 side) or back (FTO side), contributed to create higher photocurrent. As depicted in Figure 18 (b), the higher contribution was obtained when performing back illumination.

For a better understanding of the system, it was identify the chemical reactions being carried out at the photoanode by controlling the sulfur composition of the electrolyte. As shown in Table 2 treated tailings contain mainly a large concentration of sulfate and thiosulfate anions which could be the electron source, while it is expected that the cations in the treated tailings do not undergo any further electron injection reactions.

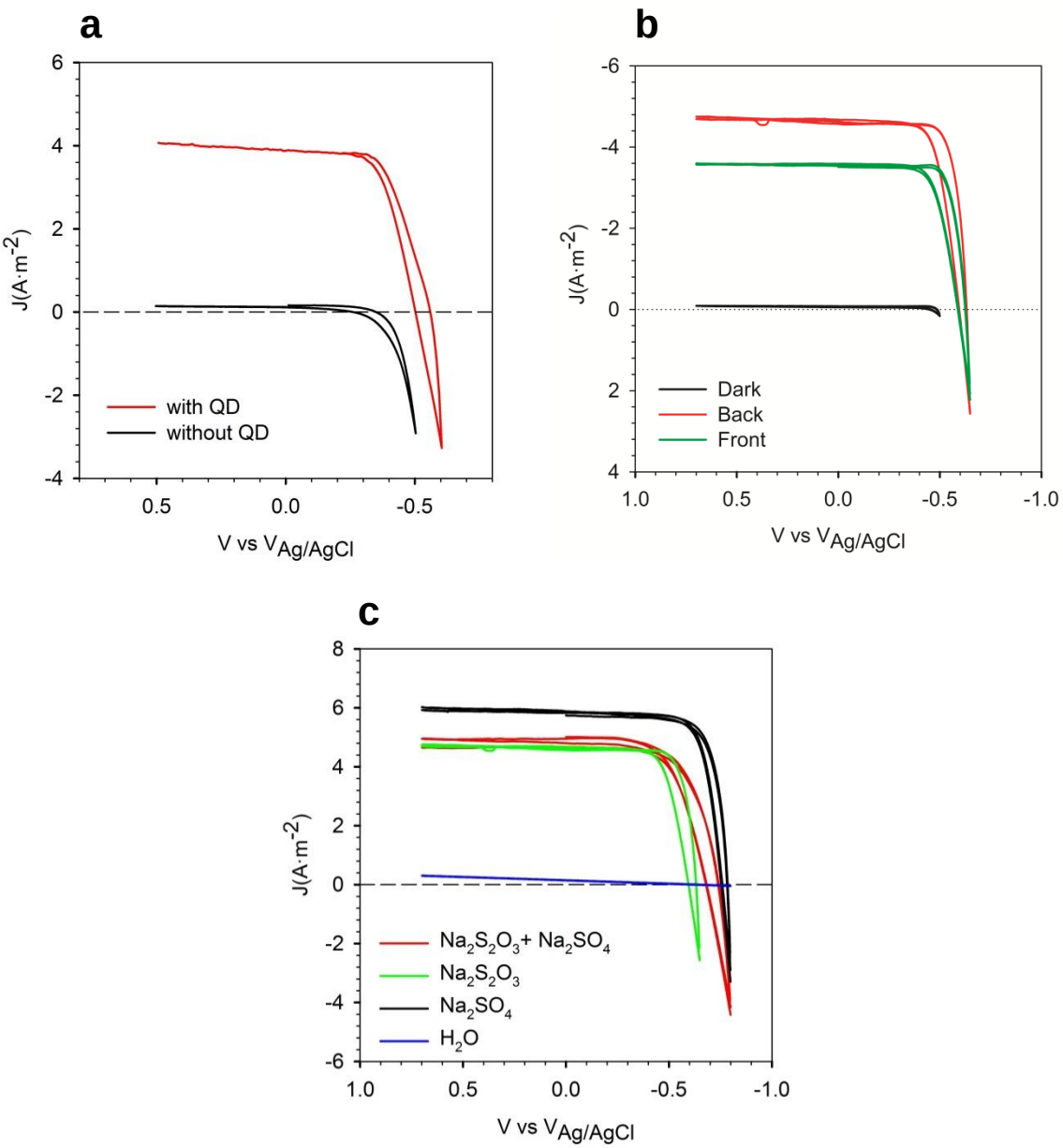

Figure 18. J-V curves of **(a)** 8.2 µm thick TiO_2 with a 40nm CL of TiO_2 samples with and without QDs **(b)** 8.2 µm thick TiO_2/QDs with a 40nm CL of TiO_2 samples illuminated front, back and in dark **(c)** 8.2 µm thick TiO_2/QDs with a 40nm CL of TiO_2 samples in respective solutions as described in legend with concentrations of 138 $mg \cdot L^{-1}$ $Na_2S_2O_3$ and 550 $mg \cdot L^{-1}$ Na_2SO_4.

Therefore, CV measurements were carried out in a 3-electrode configuration with only water (to check there are not taking place water splitting), thiosulfate or sulfate anions with the same concentration as the treated tailings. Then, both anions were combined to emulate tailing water. Results are shown in Figure 18 (c). It was observed that the J_{sc} in the case of thiosulfate solution was $1.5 A \cdot m^{-2}$ lower than the average J_{sc}

obtained in tailings, whereas the J_{sc} in the case of sulfate solution was almost the same as the average J_{sc} in tailings. The larger current in the case of sulfate solution may be associated to the higher concentration (x4) of sulfate anions as compared to thiosulfate anions rather than faster kinetics of this reaction. Table 3 presents the proposed reactions that can take place at the photoanodes.

Table 3. Proposed reactions at the anode.

Half reaction	V vs $Ag^+/AgCl$
$S_2O_3^{2-} + 6OH^- + 4h^+ \rightarrow 2SO_3^{2-} + 3H_2O$	-0.79[31]
$SO_4^{2-} + 2h^+ + 2\ OH^- \rightarrow SO_3^{2-} + ½\ O_2 + H_2O$	-0.93
$2SO_4^{2-} + 2h^+ \rightarrow S_2O_3^{2-} + 2\ O_2 + H_2O$	See reference[32]
$SO_4^{2-} + 4H_2O + 2e^- \rightarrow SO_3^- + 2OH^-$	-1.13

3.2. Photoelectrochemical cell optimization

With the aim to optimize the system, two different factors were studied: the effect of the series resistance and the thickness of the TiO_2 mesoporous layer.

3.2.1. Effect of series resistance

EIS experiments were carried out in order to minimize the effect of the series resistance (R_{series}). Taking into account that R_{series} can mainly be affected by the electrolyte conductivity, the distance between electrodes and the charge transfer at the cathode, experiments modifying such parameters were designed.

As show Figure 19 (a) non-optimized system (black line) had a very high series resistance (R_{series}= 745.7Ω), while after optimizing the system (red line), by reducing electrodes distance and increasing conductivity of electrolyte (from 2mS/cm^2 to 10mS/cm^2), the series resistance was reduced to 238.5Ω

In Figure 19 (b) sample with low resistance shows a small arc at high frequency, associated to charge transfer at the cathode. On the contrary, for cell with high resistance, high frequency arc is much larger. The differences between these two samples in this arc where attributed to the use of FTO glass in the high resistance while in the low resistance sample, FTO was substituted by a large area graphite electrode.

In the CV Figure 19 (c) it is possible to see how the total series resistance affects the slope of the graph: the low series resistance device (red line) has more slope than the high series resistance cell (black line), yielding to higher FF and better efficiency in the first case.

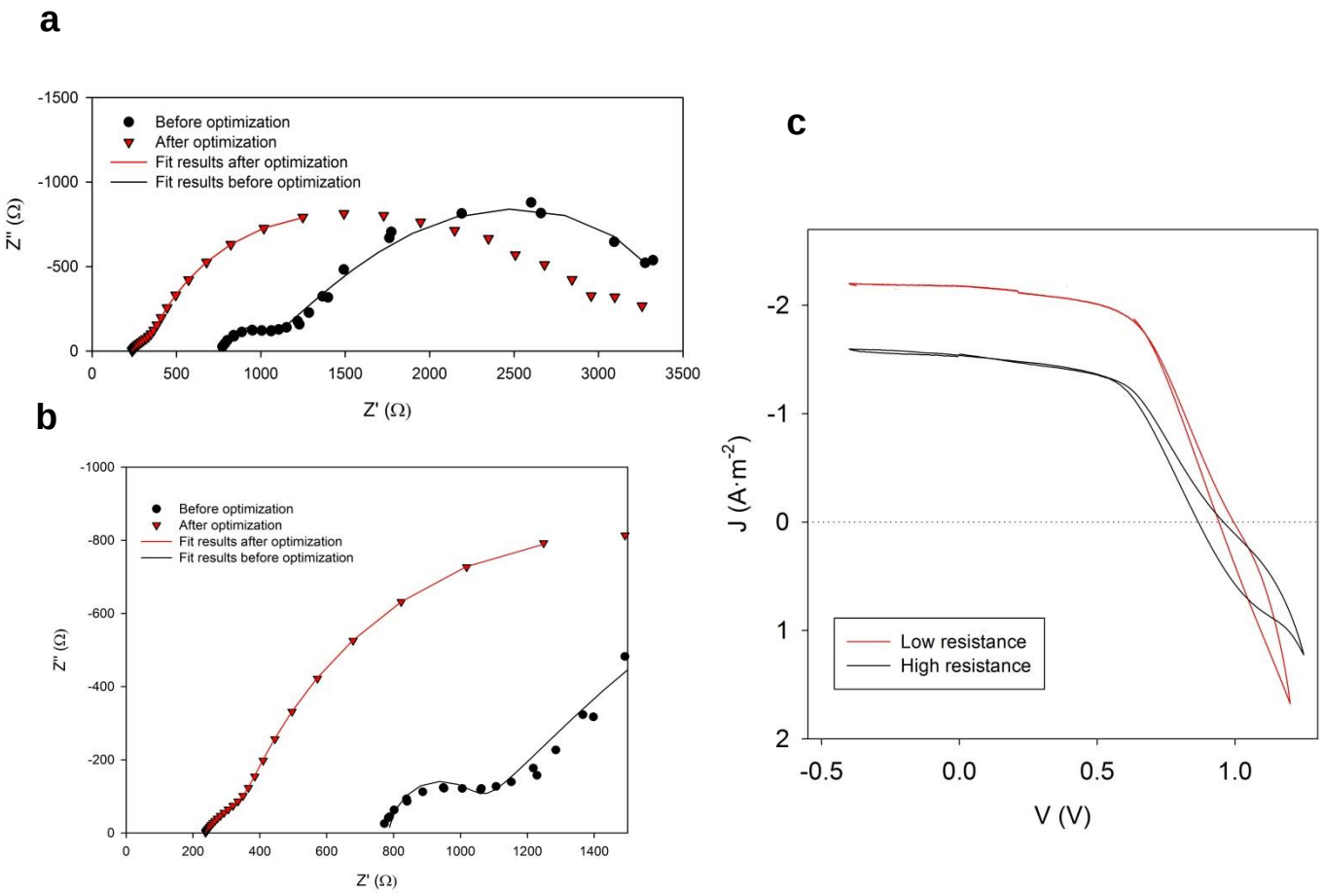

Figure 19. (a) and **(b)** EIS of 8.2 µm thick TiO_2/QDs with a 40nm CL of TiO_2 samples **(c)** Series resistance influence in CV of 8.2 µm thick TiO_2/QDs with a 40nm CL of TiO_2 samples.

In order to avoid the effect of series resistance due to the distance between electrodes, a new PEC, as shown in Figure 20, was designed. Experiments with this novel PEC are still under development

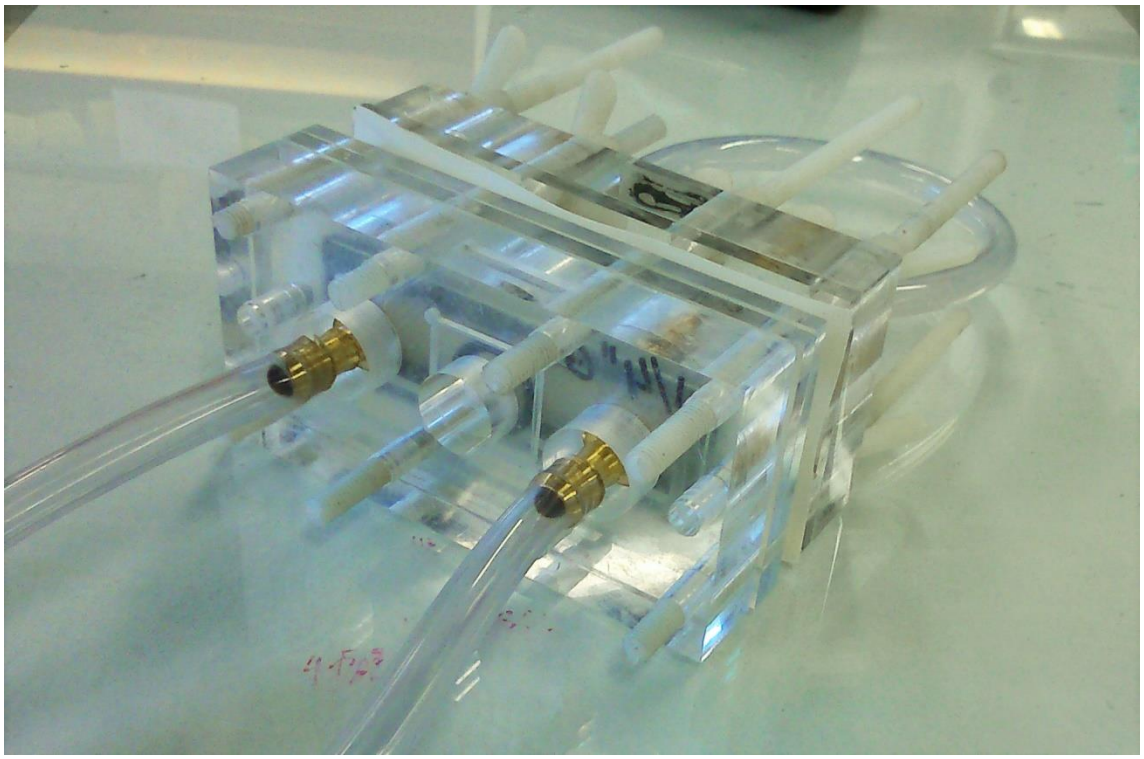

Figure 20. PEC designed to avoid the series resistance due to distance between electrodes.

3.2.2. Effect of varying TiO_2 layer thickness

After demonstrating the operation of PEC, the next step involved the optimization of the performance. In order to achieve this goal, two different procedures were followed. First, different thickness of the TiO_2 mesoporous layer were studied, as the amount of QDs absorbed and consequently the current produce depends on this parameter. Secondly, electrodes without TiO_2 compact layer were prepared (FTO/TiO_2 mesoporous/QDs) with the aim to check if the recombination at the FTO/electrolyte interface could be reduced, thus improving the electron injection from TiO_2 nanoparticles to the FTO.[33]

CV measurements for FTO/TiO_2 CL/TiO_2 mesoporous/QDs samples are shown in Figure 21 (a). It can be observed an increase in performance with the thickness of the mesoporous TiO_2 layer. In the case of electrodes without TiO_2 CL, the performance was lower, as observed in Figure 21 (b). This result indicates that the role of the TiO_2 CL is to avoid the recombination by a back-reaction, i.e.: electron transfer from FTO to the solution at the FTO/electrolyte/TiO_2, as reported for the case of dye-sensitized solar cells.[34-36]

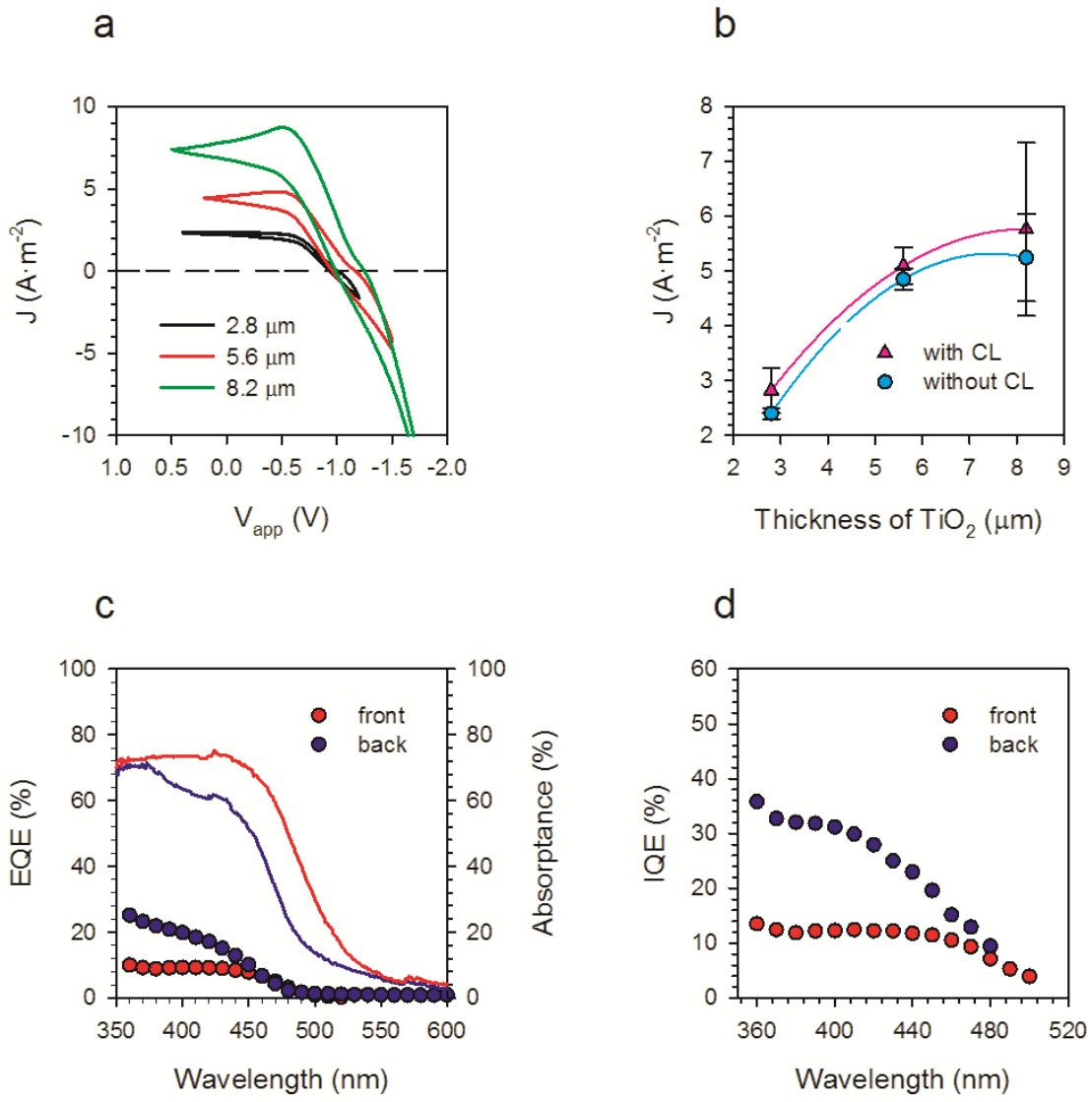

Figure 21. (a) CV measurements for TiO_2/QDs sample with a 40 nm CL of TiO_2. varying thicknesses of mesoporous TiO_2 **(b)** Variation of average short-circuit current density with 8.2 µm thick TiO_2/QDs with and without a 40nm CL of TiO_2 samples TiO_2 **(c)** EQE spectrum for an 8.2 µm thick TiO_2/QDs sample with a 40 nm CL of TiO_2.obtained from FTO side illumination (back) and TiO_2/QD side illumination (front). Solid lines represent respective absorptance for front and back illumination. **(d)** IQE spectra for front and back illumination of 8.2 µm thick TiO_2/QDs sample with a 40 nm CL of TiO_2.

To shed light on some of the operational properties of the cell, EQE measurements were performed over samples with average performances of the order of J_{sc} ~ 4.8 $A \cdot m^{-2}$, shown in Figure 21 (c). The onset of the EQE occurs at 500 nm whereas the absorption onset is at 470 nm. This indicates that injection from the QDs to TiO_2 is inefficient between the absorption onset and absorption plateau, which also corresponds to the EQE onset. The difference of 10 perceptual points between EQE

obtained under front and back illumination is associated to a diffusion length shorter than the thickness of the film. Illumination from the FTO (back) side allows the electrons to be generated closer to the contact for an easier extraction as compared to front illumination where the electrons are required to diffuse almost the entire length of the film before extraction. Corresponding internal quantum efficiency (IQE) plots in Figure 21 (d) confirm that both processes take place, i.e. electron diffusion length limitation for the samples and injection limitation from the QDs to the TiO_2 in the 500-570 nm wavelength range.

It is worth mentioning that the differences in absorption spectra for front and back illumination are due to the higher reflectance from FTO upon back illumination as compared to front illumination, as shown in Figure 22. Associated to this, reflectance measurements in Figure 22 (b) show that reflectance is much smaller for front illumination than from back illumination. An important part of this difference is associated to light reflection at the FTO electrode.

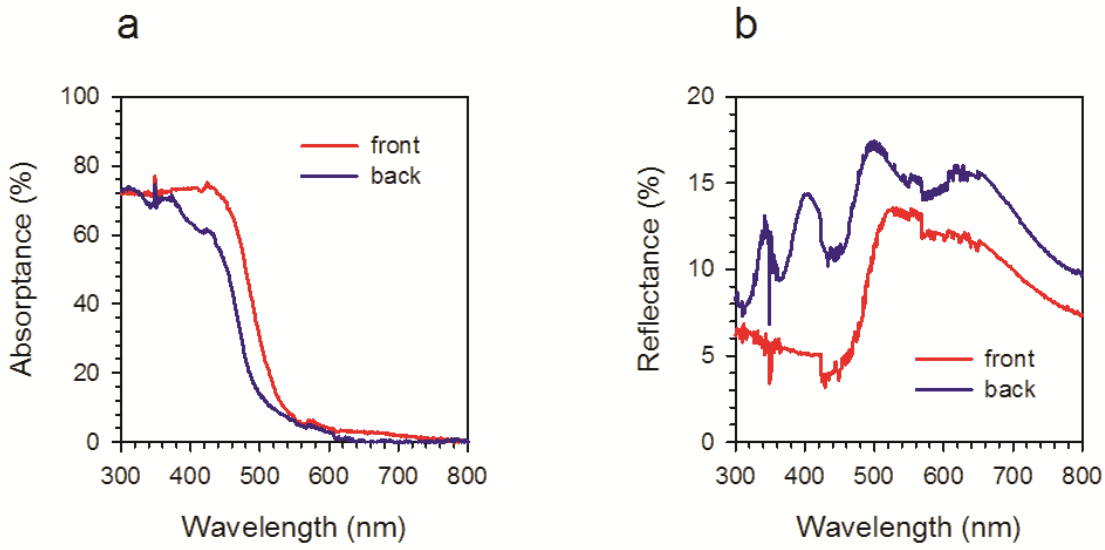

Figure 22. (a) Absorptance and **(b)** reflectance spectra of 8.2 µm thick TiO_2/QDs sample with a 40 nm CL of TiO_2 by FTO (back) side and TiO_2 (front) side illumination.

From these results, it can be concluded that although the improvement of the performance is correlated to the thickness of the mesoporous TiO_2 layer, which allows depositing more QDs, this thickness may also provokes an increase of the loss of carriers by recombination when its value is comparable or exceeds the diffusion length of the electrons.

After obtaining the optimum thickness required for highest performance, it was proceeded to optimize and identify the average performance of the 8.2µm samples with a 40 nm compact layer over a number of different samples, as shown in Figure 23. The average of J_{sc} was 6.57A·m^{-2} and an average of V_{oc} was 0.94V in a 2-electrode configuration for the 8.2µm thick samples. The highest V_{oc} obtained was 1.13V and the highest J_{sc} was 7.4A·m^{-2}. The average power that could be obtained with this device was an impressive 2.3W·m^{-2} providing a maximum power density of 3.0W·m^{-2} at a potential of 0.59V.

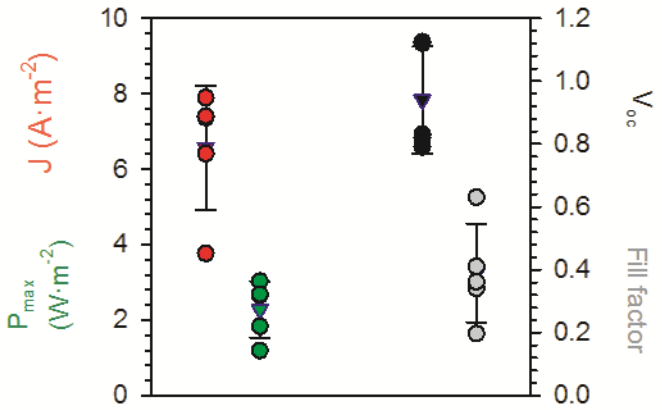

Figure 23.J_{sc}, V_{oc}, P_{max} and FF of several of 8.2µm thick TiO_2/QDs sample with a 40nm CL of TiO_2. Triangles represent average values

The obtained maximum power density for this system is also an order of magnitude higher than that reported for MFCs, which yielded maximum power densities of a few hundred mW·m^{-2} for wastewater decontamination.[37-42]

3.3. Chronoamperometry

Chronoamperometry measurements were also carried out in order to estimate the amount of Cu recovered from the solution, shown Figure 24 (a). The amount of Cu recovered at the cathode from the solution was calculated to be 0.13mg·cm^{-2} in 2.2 hours. It is possible to observe the recovered copper in Figure 24 (b).

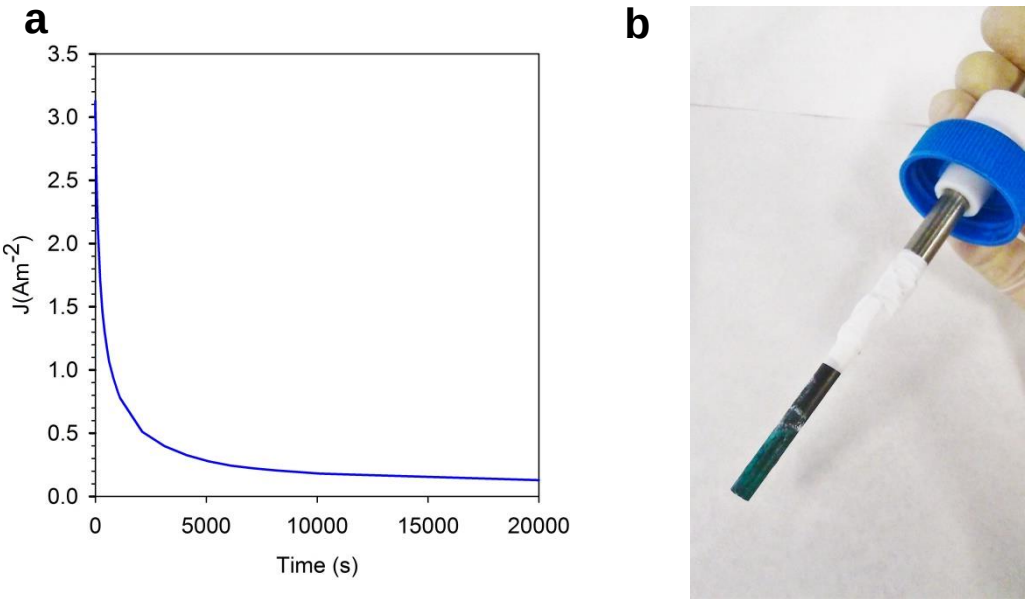

Figure 24. (a) Chronoamperometry measurement of 8.2µm thick TiO_2/QDs sample with a 40nm CL of TiO_2 **(b)** Image of amount copper recovers in cathode.

The analysis of these results suggests that the current could decrease due to a possible degradation of QDs. In order to elucidate this observation, SEM images and Microanalysis were performed to the electrodes before and after being used in chronoamperometry. These experiments are explained in section 3.4.

3.4. Scanning Electron Microscopy analysis

Figure 25 shows a SEM image of 8.2µm thick TiO_2/QD sample before being used in chronoamperometry, where is shown the mesoporous TiO_2 particle size (over 20nm).

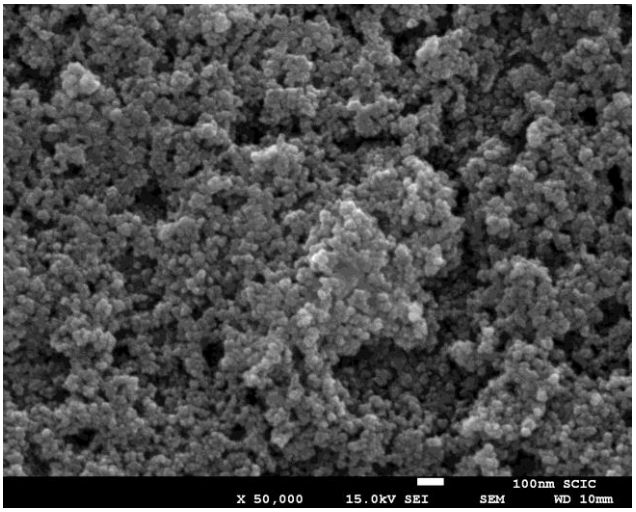

Figure 25. SEM image of 8.2 µm thick TiO_2/QDs sample with a 40 nm CL of TiO_2.

A qualitative analysis of the degraded and non-degraded samples was performed. Figure 26 shows the elements mapping by EDS (Energy Dispersive X-Ray Spectrometry) of the different samples.

a b

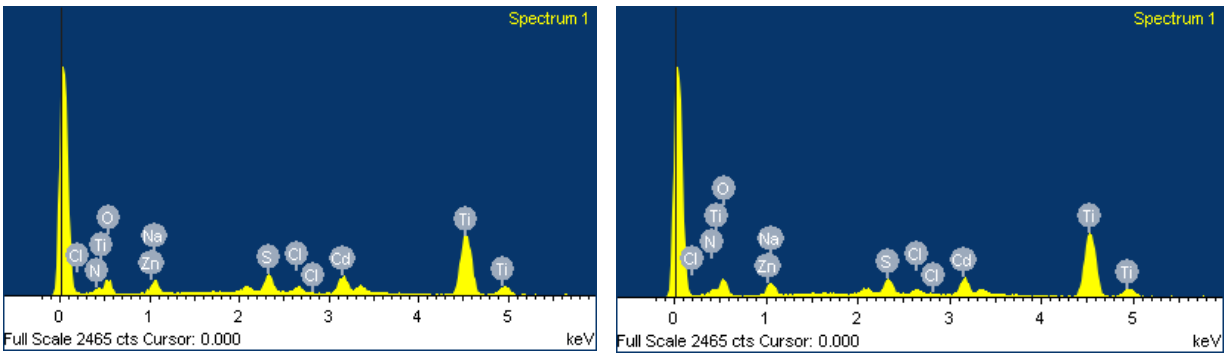

Figure 26. Microanalysis **(a)** before and **(b)** after chronoamperometry of 8.2µm thick TiO_2/QDs sample with a 40 nm CL of TiO_2

Table 4 shows the microanalysis of elements presents in non-degraded and degraded samples and the atomic differences between each element present in samples.

Table 4. Microanalysis of samples before and after chronoamperometry.

Element	Non-degraded	Degraded	Differences
	Atomic%	Atomic%	Atomic
O	66.74	65.33	-1.41
Na	0.00	3.36	3.36
S	3.32	3.69	0.37
Cl	1.26	1.30	0.04
Ti	23.19	21.38	-1.81
Zn	2.45	1.47	-0.98
Cd	3.05	3.48	0.43

As shown in Table 4, degraded samples have smaller values for zinc and titanium than fresh samples. Also, sodium from the solution appears in sample after chronoamperometry. This result suggests that sodium replaces zinc and titanium and this is the origin of QDs degradation during chronoamperometry. If it occurs, ZnS is

being degraded causing a depassivation of surface states of the core and, consequently, a higher recombination of the electron-hole pairs photogenerated.

Chapter 4: Conclusions

In conclusion, this works presents the proof of concept for new photoelectrochemical cells that may be applied to generate energy at the same time that decontaminates water and recovers metals from solution. This system is based on CdS QD sensitized TiO_2 photoanodes which carry out sulphur oxidation reactions in heavy metal-free tailings water with simultaneous recovery of Cu in a cathode immersed in Cu-rich tailings.

The highest open circuit voltage was 1.13V and the highest short-circuit current density was $7.4 A \cdot m^{-2}$ for an 8.2µm thick sample with a 40nm thick CL of TiO_2. The maximum power density was $3.0 W \cdot m^{-2}$, one order of magnitude higher than that obtained by microbial fuel cells for wastewater treatment. This system can be used in tandem with bioleaching processes for efficient Cu recovery, allowing for economic viability due to the simultaneous generation of electric power.

Despite the low power generated by the PEC studied in this project, this system has a great potential as it can resolve the two main problems associated with mining: (i) the need of mine industry to have a low cost alternative for tailings treatment that will follow the increasing restrictive regulations and reduce the space needed to store the waste and (ii) the simultaneous production of high purity copper with no energy cost.

Besides, it has also been demonstrated that the cells developed does not suffer from any of the problems that have limited the progress of MFC on an industrial level for wastewater applications i.e.: high internal resistances[43] and requirement of a mediator to transfer electrons from the microbes to the anode.[44]

Therefore, this system provides features that overcome the state of the art of the current technologies for metal recovery and water decontamination, i.e.: bioleaching plus electro-wining or microbial fuel cells. The use of bioleaching in tandem with this system to recover solubilized copper can help to make exploitation of low grade mineral ores more economically viable for industrial applications due to the simultaneous generation of electric power.

References

1. D. Grey, D. Garrick, D. Blackmore, J. Kelman, M. Muller and C. Sadoff, *Philosophical Transactions of the Royal Society of London A: Mathematical, Physical and Engineering Sciences*, 2013, **371**.
2. P. M. Heikkinen, M. L. Räisänen and R. H. Johnson, *Mine Water and the Environment*, 2008, **28**, 30-49.
3. E. Lee, Y. Han, J. Park, J. Hong, R. A. Silva, S. Kim and H. Kim, *Journal of Environmental Management*, 2015, **147**, 124-131.
4. P. Eck and L. Wilson, *Eck Institute of Applied Nutrition and Bioenergetics, Ltd., Phoenix, AZ*, 1989, **4**.
5. EU, 2006.
6. M. A. Barakat, *Arabian Journal of Chemistry*, 2011, **4**, 361-377.
7. H. A. Hegazi, *HBRC Journal*, 2013, **9**, 276-282.
8. J. G. Dean, F. L. Bosqui and K. H. Lanouette, *Environmental Science & Technology*, 1972, **6**, 518-522.
9. L.-J. Zhang, H.-C. Tao, X.-Y. Wei, T. Lei, J.-B. Li, A.-J. Wang and W.-M. Wu, *Chemosphere*, 2012, **89**, 1177-1182.
10. H. V. Hamelers, A. Ter Heijne, T. H. Sleutels, A. W. Jeremiasse, D. P. Strik and C. J. Buisman, *Applied microbiology and biotechnology*, 2010, **85**, 1673-1685.
11. A. T. Heijne, F. Liu, R. v. d. Weijden, J. Weijma, C. J. N. Buisman and H. V. M. Hamelers, *Environmental Science & Technology*, 2010, **44**, 4376-4381.
12. J. Luo, L. Ma, T. He, C. F. Ng, S. Wang, H. Sun and H. J. Fan, *The Journal of Physical Chemistry C*, 2012, **116**, 11956-11963.
13. P. Sudhagar, V. Gonzalez-Pedro, I. Mora-Sero, F. Fabregat-Santiago, J. Bisquert and Y. S. Kang, *Journal of Materials Chemistry*, 2012, **22**, 14228-14235.
14. H. B. Yang, J. Miao, S.-F. Hung, F. Huo, H. M. Chen and B. Liu, *ACS Nano*, 2014, **8**, 10403-10413.
15. H. Grahn, *Introduction to Semiconductor Physics* 1999.
16. H. P. Rocksby, 1932, 16, 171.
17. A. I. Ekimov, A. L. Efros and A. A. Onushchenko, *Solid State Communications*, 1985, **56**, 921-924.
18. E. Borovitskaya and M. Shur, *Quantum Dots*, World Scientific, 2002.

19. V. A. Jef Poortmans, 2006.

20. P. V. Kamat, *The Journal of Physical Chemistry C*, 2007, **111**, 2834-2860.

21. T. Torchynska and Y. Vorobiev, *Semiconductor II-VI Quantum Dots with Interface States and Their Biomedical Applications*, INTECH Open Access Publisher, 2011.

22. L. Cademartiri, E. Montanari, G. Calestani, A. Migliori, A. Guagliardi and G. A. Ozin, *Journal of the American Chemical Society*, 2006, **128**, 10337-10346.

23. H. Y. Wei, G. S. Wang, H. J. Wu, Y. H. Luo, D. M. Li and Q. B. Meng, *Acta Phys.-Chim. Sin.*, 2016, **32**, 201-213.

24. J. Zhang, J. Gao, E. M. Miller, J. M. Luther and M. C. Beard, *ACS Nano*, 2014, **8**, 614-622.

25. M. Tytus, J. Krasnyj, W. Jacak, A. Chuchmala, W. Donderowicz and L. Jacak, in *Symmetry and Structural Properties of Condensed Matter*, eds. T. Lulek, B. Lulek and A. Wal, 2008, vol. 104, pp. 12011-12011.

26. P. S. Patil, *Materials Chemistry and Physics*, 1999, **59**, 185-198.

27. F. C. Krebs, *Solar Energy Materials and Solar Cells*, 2009, **93**, 394-412.

28. P. T. Valeri, *Russian Chemical Reviews*, 2006, **75**, 161.

29. R. S. Liu, *Electrochemical Technologies for Energy Storage and Conversion: Vol. 1*, Wiley-VCH Verlag & Company KGaA, 2012.

30. F. Fabregat-Santiago, G. Garcia-Belmonte, I. Mora-Seró and J. Bisquert, *Physical chemistry chemical physics*, 2011, **13**, 9083-9118.

31. M. Bouroushian, *Electrochemistry of metal chalcogenides*, Springer Science & Business Media, 2010.

32. A. Bruynesteyn and R. P. Hackl, 2009.

33. M. S. Góes, E. Joanni, E. C. Muniz, R. Savu, T. R. Habeck, P. R. Bueno and F. Fabregat-Santiago, *The Journal of Physical Chemistry C*, 2012, **116**, 12415-12421.

34. H. Choi, C. Nahm, J. Kim, J. Moon, S. Nam, D.-R. Jung and B. Park, *Current Applied Physics*, 2012, **12**, 737-741.

35. A. Burke, S. Ito, H. Snaith, U. Bach, J. Kwiatkowski and M. Grätzel, *Nano Letters*, 2008, **8**, 977-981.

36. H. Yu, S. Zhang, H. Zhao, G. Will and P. Liu, *Electrochimica Acta*, 2009, **54**, 1319-1324.

37. D.-J. Lee, C.-Y. Lee and J.-S. Chang, *Journal of Hazardous Materials*, 2012, **243**, 67-72.

38. H. Moon, I. S. Chang and B. H. Kim, *Bioresource Technology*, 2006, **97**, 621-627.

39. Y. Zhang, J. S. Noori and I. Angelidaki, *Energy & Environmental Science*, 2011, **4**, 4340-4346.

40. S. Hays, F. Zhang and B. E. Logan, *Journal of Power Sources*, 2011, **196**, 8293-8300.

41. K.-Y. Kim, W. Yang and B. E. Logan, *Water Research*, 2015, **80**, 41-46.

42. Y. Ahn, M. C. Hatzell, F. Zhang and B. E. Logan, *Journal of Power Sources*, 2014, **249**, 440-445.

43. J. J. Fornero, M. Rosenbaum and L. T. Angenent, *Electroanalysis*, 2010, **22**, 832-843.

44. Z. Du, H. Li and T. Gu, *Biotechnology Advances*, 2007, **25**, 464-482.